Piezoresistive Cantilever Optimization and Applications

Joseph C. Doll, Sung-Jin Park, Nahid Harjee, Ali J. Rastegar,
Joseph R. Mallon Jr., Bryan C. Petzold, Ginel C. Hill, A. Alvin Barlian and Beth L. Pruitt
Stanford University, Stanford, CA

ABSTRACT

Piezoresistors are commonly used in microsystems for transducing force, displacement, pressure and acceleration. Silicon piezoresistors can be fabricated using ion implantation, diffusion or epitaxy and are widely used for their low cost and electronic readout. However, the design of piezoresistive cantilevers is complicated by coupling between design parameters as well as fabrication and application constraints. Here we discuss analytical models and design optimization for piezoresistive cantilevers, and describe several applications ranging from studying electron movement using scanning gate microscopy to measuring the biomechanics of whole organisms.

INTRODUCTION

Piezoresistivity, the change in resistivity of a material under stress [1], is commonly used in micro-electro-mechanical systems (MEMS) for transducing force [2, 3, 4], pressure [5, 6, 7] and acceleration [8]. The optimal sensor geometry depends upon the type of mechanical loading, but a simple cantilever beam implementation is ideal for many applications. Microfabricated silicon cantilevers are widely used in force [9, 10], topography [11], and biochemical sensing [12] applications by transducing a signal via cantilever deflection. There are numerous techniques to detect cantilever bending, but the most common approaches are off-chip optical sensing [11] and on-chip electronic sensing using piezoresistive strain gauges [13]. Electronic sensing scales well to large arrays [14], high frequencies [15], and situations where optics are inconvenient [16]. Piezoresistive sensors have several desirable characteristics including straightforward fabrication, simple signal-conditioning circuitry, compact size, and large dynamic range. With proper design, the resolution of piezoresistive cantilevers is comparable to optical detection [3, 17, 18].

Here, we provide a brief review of silicon piezoresistors with an emphasis on force sensing, discuss some aspects of design modeling and optimization, and describe several example applications from our lab. This is a survey and not a complete review of the extensive work to date by research labs spread across the globe on piezoresistors.

MODELING AND DESIGN

Principles of Piezoresistance

The electrical resistance (R) of a homogenous electrical conductor with constant cross-section can be calculated from its dimensions and resistivity according to

$$R = \frac{\rho l}{a} \tag{1}$$

where ρ is the resistivity, l is the length and a is the cross-sectional area. The resistance of the conductor changes with geometry (length and area) and resistivity (carrier mobility and density). Semiconductor resistance change is dominated by the stress-induced change in mobility and can be simplified as

$$\frac{\Delta\rho}{\rho} = \pi_l \sigma_l + \pi_t \sigma_t \tag{2}$$

where π_l and π_t are the longitudinal and transverse piezoresistive coefficients, while σ_l and σ_t are the longitudinal and transverse stress components where the piezoresistor is situated. A more thorough discussion of the history and mechanisms underlying piezoresistance in semiconductors can be found in [1].

The piezoresistive coefficients vary with dopant concentration, and experimental data has been tabulated and empirically fit by Harley [19]. The longitudinal piezoresistive coefficient can be written as $\pi_l = P\pi_0$ where $\pi_0 = 72 \cdot 10^{-11}\text{Pa}^{-1}$ for a p-type piezoresistor oriented in the $\langle 110 \rangle$ direction and P is the concentration dependent piezoresistance factor, which is equal to

$$P = \log_{10}\left(\frac{b}{n}^a\right) \tag{3}$$

where $a = 0.2014$, $b = 1.53 \cdot 10^{22}$, and n is the dopant concentration in cm^{-3}.

This expression incorrectly predicts that P increases indefinitely as n decreases, and is only accurate for dopant concentrations greater than 10^{18} cm^{-3}. The reader is referred to modeling and experimental work by Richter et al [20] for a more general but less compact expression that is accurate to low dopant concentration and includes the temperature dependence of piezoresistivity.

The longitudinal and transverse piezoresistive coefficients vary with the dopant type and the crystallographic orientation of the current flow relative to the applied stress. For a p-type dopant (e.g. boron), the direction of maximum longitudinal piezoresistive coefficient is the $\langle 110 \rangle$ direction, while for n-type dopants (e.g. phosphorus, arsenic) the optimal direction of stress and current is the $\langle 100 \rangle$ direction. As noted earlier, the piezoresistance coefficients also depend on temperature [20], and the effect of temperature fluctuations on the output signal is commonly reduced by including an additional temperature compensation piezoresistor in the measurement circuit which can be unstrained [10] or strained [21].

Force and Displacement Sensitivity of a Cantilever Beam

In this section we specifically investigate the sensitivity of a split-leg cantilever beam, which is well suited for force detection but can be adapted for displacement, inertial or surface stress detection.

In a split-leg cantilever design, two separate legs each of length l_{pr} and width $w_{pr} = w/2$ form a loop to define the piezoresistor. The cantilever extends beyond the end of the piezoresistor to a total length l. The thickness, t, is uniform along the length. The gap between the legs is assumed to be negligibly wide, and the cantilever can be approximated to have a uniform width w. The dimensions and one of many possible microfabrication processes to form a cantilever are illustrated in Figure 1.

The system is modeled as a linear elastic cantilever beam with a point load applied at the tip via Euler-Bernoulli beam theory. However, finite element analysis could be used to incorporate second order effects such as transverse stress and the anisotropic mechanical properties of silicon. We assume negligible transverse stress in the cantilever legs, and the longitudinal stress induced as a function of distance x from the base and z from the neutral axis of the cantilever is

$$\sigma = \frac{12F(l-x)z}{wt^3}. \tag{4}$$

The longitudinal stress induced by a point load is assumed zero at the neutral axis, and varies linearly through the cantilever thickness, thus the stress experienced by the piezoresistor varies by position along both the x- and z-axes. It is worth noting that for some devices the neutral axis of the beam may not coincide with the centroid of the beam due to non-negligible metal or dielectric thin films deposited on the surface, particularly for thin cantilever beams.

If the piezoresistor is uniformly doped, infinitely thin, and located at the surface of the cantilever where the stress is maximized, the fractional change in resistance is

$$\frac{\Delta R}{R} = \frac{6\pi_l(l-l_{pr}/2)}{wt^2}F \tag{5}$$

as derived previously [23]. In practice, these assumptions overpredict cantilever sensitivity due to the finite thickness of the piezoresistor. An efficiency factor, β^*, accounts for the finite thickness

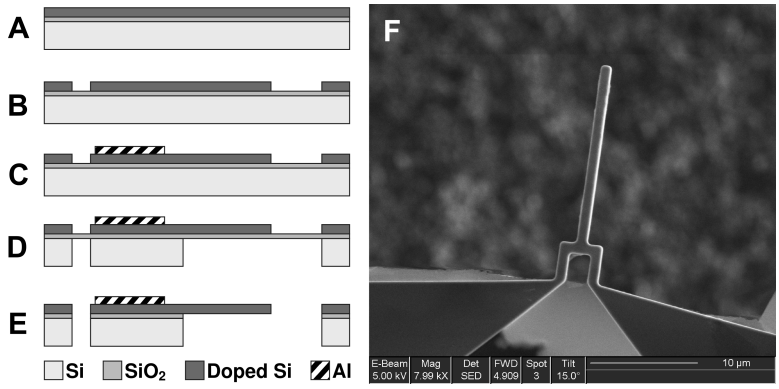

Figure 1: Piezoresistive cantilevers are commonly fabricated using silicon-on-insulator wafers in combination with standard silicon micromachining processes. After the wafer is doped (a), the cantilever is defined (b) by reactive ion etching. Aluminum is sputtered to cover the frontside of the wafer and etched back to form bondpads (c). The cantilever is released by deep reactive ion etching from the backside of the wafer (d) followed by reactive ion etching of the buried oxide (e). A forming gas anneal is necessary to form low noise, ohmic contacts. An SEM of a finished device is shown in (f). Reprinted from Doll et al. [22].

of the piezoresistor and proportionally reduces the fractional change in resistance as

$$\beta^* = \frac{2}{t}\frac{\int_{-t/2}^{t/2} q\mu nPz dz}{\int_{-t/2}^{t/2} q\mu n dz} \tag{6}$$

where the majority carrier mobility, μ, and weighted piezoresistive coefficient, P, are both functions of dopant concentration, n, which varies with depth, z [24]. In the case of a uniformly doped piezoresistor with finite thickness t_{pr}, β^* simplifies to

$$\beta^* = P(1 - \frac{t_{pr}}{t}). \tag{7}$$

A simplified form, β was first derived by Tortonese [13] for epitaxial, uniform doping and was extended later to address dopant profiles with varying concentration [24].

A Wheatstone bridge is commonly used to transduce the change in resistance to a voltage. A bridge reduces the sensitivity in the case that only one of the resistors in the bridge is located on the cantilever beam (quarter-active, $V_{out}/V_{bridge} \approx \Delta R/4R$). However a Wheatstone bridge is simple to implement, uses only passive components so can have low-noise, and the signal conditioning electronics can be situated far away from the sensor by using an instrumentation amplifier with a high common-mode rejection ratio. For our sensitivity and noise calculations that follow, we assume a quarter-active Wheatstone bridge with an additional unstrained temperature compensation silicon resistor. The overall voltage sensitivity is given as

$$S_F = \frac{\Delta V}{F} = \frac{3\pi_0(l - l_{pr}/2)}{2wt^2} V_{bridge}\beta^*\gamma \tag{8}$$

where γ is the ratio of the piezoresistor resistance to the total resistance measured. Resistance that does not contribute to the change in resistance with applied force, such as contact resistance and conducting traces, acts to reduce system sensitivity and increase noise. The sheet resistance of doped silicon is almost always much larger than an aluminum trace, so γ can be made approximately equal to 1 with careful design.

Noise in Piezoresistors

Piezoresistive cantilever performance is limited by two primary sources of noise: Johnson and 1/f (Hooge) noise [3, 2]. The noise inherent to signal conditioning circuitry (e.g. Johnson and 1/f noise of the amplifier) must considered as well and sets a noise floor for the piezoresistor.

Johnson noise is the result of the thermal motion of carriers within a resistive element and is independent of frequency [26]. The Johnson noise of a balanced Wheatstone bridge is equal to the Johnson noise of a single resistor ($R/2$ seen by each input of the instrumentation amplifier), so that the integrated Johnson noise power of the Wheatstone bridge in the frequency band f_{min} to f_{max} is

$$\overline{V_J^2} = 4k_bTR(f_{max} - f_{min}). \tag{9}$$

The piezoresistor resistance (R) can be calculated from the dopant concentration profile and corresponding sheet resistance. Variation in carrier mobility with concentration should be considered [27]. For a sheet resistance of R_s, $R \approx 2R_s l_{pr}/w_{pr}$.

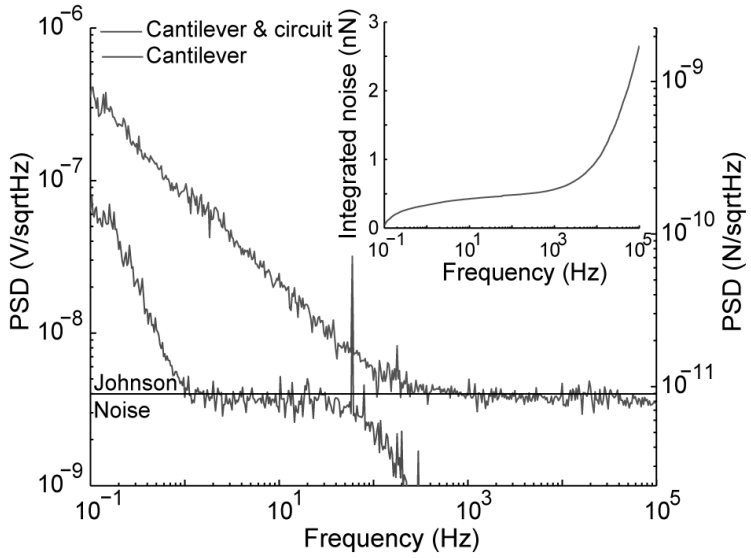

Figure 2: Noise power spectral density (PSD) for a cantilever and associated conditionining circuitry, which illustrates the contributions of Johnson and low frequency noise from various sources. Inset: integrated noise from 0.1 Hz. Reprinted from Park et al. [25]. ©2009 IEEE.

The primary 1/f noise source in silicon piezoresistors is Hooge noise [3]. The voltage power spectral density of a single piezoresistor has been empirically modeled as

$$\overline{S_H^2} = \frac{\alpha V_{bias}^2}{Nf} \tag{10}$$

where $V_{bias} = V_{bridge}/2$ is the piezoresistor bias voltage, N is the total number of carriers in the resistor, and f is the frequency [28] . The parameter α is an experimentally measured value that is believed to depend upon crystal lattice quality. Ion implantation causes damage to the crystal lattice that must be annealed out, and researchers have observed that α decreases with the mean diffusion length ($\sqrt{Dt}$) of the dopant atoms during the anneal [3]. For epitaxial piezoresistors, $\alpha = 10^{-5}$ is typical [19] although values of α as low as 10^{-7} have been reported for implanted piezoresistors [21].

Our Wheatstone bridge is composed of two piezoresistors which are uncorrelated 1/f noise sources, so the 1/f noise power is increased by a factor of two, and the integrated voltage noise power is

$$\overline{V_H^2} = \frac{\alpha V_{bridge}^2}{2N} \ln\left(\frac{f_{max}}{f_{min}}\right). \tag{11}$$

The number of carriers can be calculated from the dopant concentration profile and piezoresistor volume assuming a constant current density [19]. For a piezoresistor with N_z carriers per unit area, $N \approx 2 l_{pr} w_{pr} N_z$.

Force Resolution and Design Tradeoffs

The minimum resolvable force can be calculated from the root mean square voltage noise and the force sensitivity of the device according to

$$F_{min} = \frac{\overline{V_{noise}}}{S_F} = \frac{\sqrt{\frac{\alpha V_{bridge}^2}{4 l_{pr} w_{pr} N_z} \ln(\frac{f_{\max}}{f_{\min}}) + 8 k_B T R_s \frac{l_{pr}}{w_{pr}} (f_{\max} - f_{\min})}}{\frac{3(l-0.5 l_{pr})\pi_0}{2wt^2} \gamma V_{bridge} \beta^*}. \tag{12}$$

Force resolution is affected by several factors: cantilever dimensions (l, w, t), piezoresistor dimensions (l_{pr}, w_{pr}, γ), fabrication process parameters (N_z, R_s, α, β^*, γ), and operating parameters (V_{bridge}, T, $f_{\min}$, $f_{\max}$). The integrated noise and force resolution of an example piezoresistive cantilever are shown in Figure 2.

Force resolution improves with power dissipation, which can be shown by dividing the numerator and denominator of (12) by V_{bridge} to obtain

$$F_{\min} = \frac{\sqrt{\frac{\alpha}{4 l_{pr} w_{pr} N_z} \ln(\frac{f_{\max}}{f_{\min}}) + k_B T \frac{1}{W} (f_{\max} - f_{\min})}}{\frac{3(l-0.5 l_{pr})\pi_0}{2wt^2} \gamma \beta^*}, \tag{13}$$

where W is power dissipated in the piezoresistor ($V_{bridge}^2/4R$). It is clear that force resolution can be improved by increasing W to the point where Johnson noise is negligible. However, there is a limit to the maximum power dissipation sustainable by the cantilever because Joule heating can destroy the piezoresistor and large bias voltages lead to large leakage currents.

The piezoresistor length ratio and performance can be calculated for a variety of process conditions in order to find the optimal design, as in [18]. A notable result from our optimization work is that the integrated Johnson and 1/f noise should be comparable ($\overline{V_J} \approx \overline{V_H}$) for typical design conditions and constraints. Alternatively, the optimized design can be found numerically as in [17], which provides a convenient interface for the designer and can handle arbitrary nonlinear constraints.

APPLICATIONS

Force Sensors

Piezoresistive cantilevers are well-suited for the study of biomechanics at the microscale; they cover the relevant range of forces (pN to 100 μN), displacements (nm to 10 μm), and offer sufficient bandwidth (10s to 100s of kHz). We have used piezoresistive cantilevers to investigate two fundamental issues related to touch sensation in the nematode *C. elegans*: body mechanics [10, 29] and the behavioral touch threshold [25]. *C. elegans* is a model organism for genetics studies, including the study of mechanotransduction, the conversion of mechanical energy into biomechanical signals.

In the first two studies, we used a piezoresistive cantilever to apply microscale forces to the nematode and develop a model for the mechanical structure of the body wall (Figure 3) and the contribution of muscle tone to the measured stiffness. In the behavioral study, piezoresistive cantilevers were used to measure the minimum force detectable by wild-type *C. elegans* (Figure 3).

By integrating the cantilever with a fast real-time controller, we developed a MEMS force-clamp system for applying user-defined force profiles (e.g. step, sinusoidal) to *C. elegans*. Using the system, we measured a touch sensation threshold ten times smaller than accesible with previous tools.

Piezoresistive cantilevers are particularly well suited for high frequency force sensing. The cantilever dimensions are limited only by fabrication constraints and force resolution continuously improves as dimensions are reduced. By using electronic rather than optical readout, the size of the cantilever can be made arbitrarily small, enabling low stiffness and high bandwidth probes. We fabricated 340 nm thick piezoresistive cantilevers doped by $POCl_3$ diffusion, yielding pN force resolution with a measurement bandwidth up to 100 kHz [22].

Piezoresistors have been used to sense lateral or 'in-plane' forces in a micro-accelerometer [31] and underwater shear stress sensor [32]. Lateral piezoresistive sensors can be fabricated with ion implantation or epitaxy [33] and are typically located on vertical sidewalls in devices. Simultaneous sensing of two components of force has been demonstrated in cantilevers that combine sidewall piezoresistors with those oriented on a more usual top surface (Figure 4) [30]. Such dual-axis force sensors have been employed in data-writing applications and biomechanics studies of complex adhesion mechanisms [34].

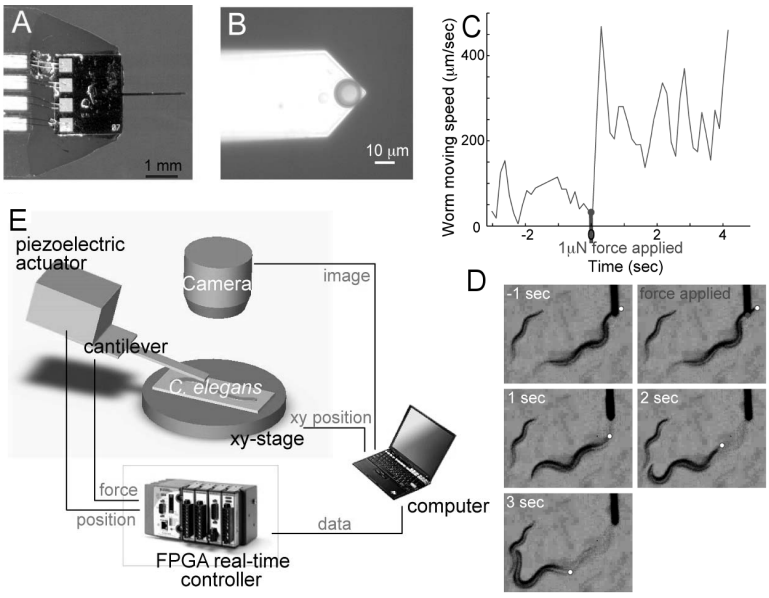

Figure 3: Piezoresistive microcantilever (2 mm long, 30 μm wide, 7 μm thick) glued on printed circuit board (a) with a 10 μm diameter glass bead on the tip to provide a controlled contact geometry (b). A 1 μN force applied to *C. elegans* induces a change in velocity (c), measured using a behavior tracking and force application system (d). A schematic of the force and displacement clamp system using proportional-integral-derivative (PID) field programmable gate array (FPGA) controller is also shown (e). Reprinted from Park et al. [25]. ©2009 IEEE.

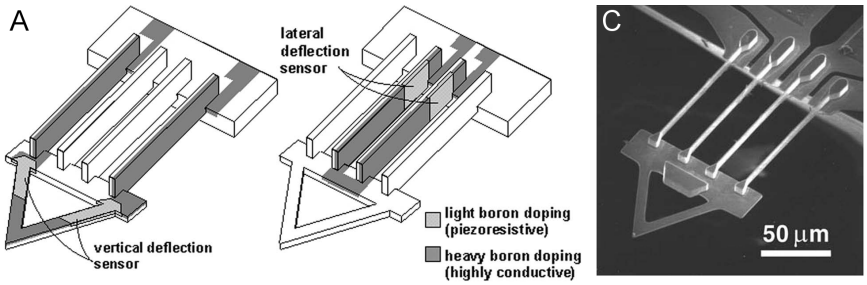

Figure 4: (A) Dual-axis piezoresistive AFM cantilever with orthogonal axes of compliance. Oblique ion implants are used to form electrical elements on vertical sidewalls and horizontal surfaces simultaneously. (B) SEM image of a fabricated device. Reprinted with permission from Chui et al. [30]. ©1998 American Institute of Physics.

Scanning Probe Microscopy

Atomic force microscopy (AFM) with piezoresistive cantilevers was first demonstrated by Tortonese et al. [13]. Measurement of tip deflection via piezoresistive transduction has two advantages over the conventional laser beam bounce technique. First, the system setup is compact and inexpensive, enabling applications in space-constrained environments (for example, on upright or inverted microscopes or in cryostats). Second, because piezoresistive cantilevers do not require a laser, samples are not susceptible to optical excitation, an important consideration in techniques such as scanning gate microscopy (SGM) [36].

In AFM, we are interested in optimizing the minimum resolvable tip displacement, d_{min}. Dividing (12) by k, the spring constant of the cantilever, we obtain an expression for d_{min}. By increasing k, we can improve the displacement resolution. Many scanning probe techniques are performed at liquid He temperatures (4.2K and below). Noise is greatly reduced for piezoresistive cantilevers operated in these conditions. Instead, power dissipation becomes a key design parameter as the

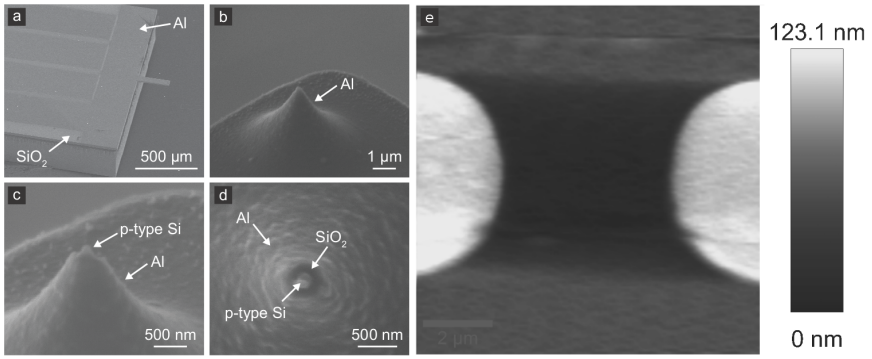

Figure 5: Scanning electron micrographs of a fabricated scanning probe: (a) 1.6 mm x 3.6 mm die featuring a 3 μm thick x 50 μm wide x 255 μm long silicon cantilever with implanted BF_2 piezoresistor and inner conductor, SiO_2 insulator and Al electrodes and shield; a 3 μm tall coaxial tip (b) before FIB (oblique) and after FIB from (c) oblique and (d) top views. FIB opening in Al/SiO_2 at tip apex is 100 nm in radius. (e) AFM image of Au electrodes on SiO_2. Z-axis height controlled by piezoresistive feedback. Reprinted from Harjee et al. [35]. ©2010 IEEE.

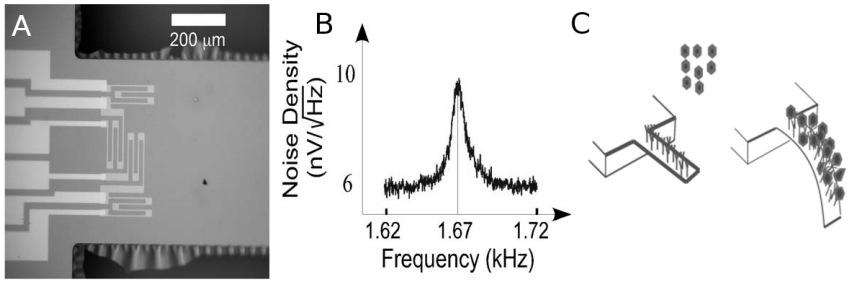

Figure 6: (A) Silicon microcantilever, 3.5 mm long, 0.65 mm wide, and 15 μm thick with transverse and longitudinal piezoresistors. (B) Self-sensed thermomechanical noise spectral density for one of the fabricated cantilevers. (C) The cantilever surface can be functionalized to detect chemical binding induced surface stress, yielding a chemical sensor capable of operation in liquid. Reprinted with permission from Mallon et al. [21]. ©2008 American Institute of Physics.

cooling power of most dilution refrigerators is in the order of tens of microwatts.

With the considerations above, we have fabricated piezoresistive cantilevers with integrated coaxial tips [35]. The probes can image nanometer topography in a 10 kHz bandwidth and the tips can generate tightly-confined electric field perturbations for high-resolution SGM (Figure 5).

Chemical Sensors

A functional chemical layer deposited on the surface of a cantilever can be used for chemical sensing by surface stress change induced cantilever deflection [37]. Cantilevers have been used for detecting DNA [38], pH [39] and explosives [37]. Piezoresistive sensors are especially well suited to this task, because they are small, low power, have a relatively stable DC response, especially if temperature compensated [16]. Additionally, several cantilevers may be formed into an array. If each layer has varying response to chemical species, both the type and concentrations of the constituent chemical species present may be determined by factor analysis. Silicon cantilevers should be as short and as wide as possible take advantage of the transverse piezoresistive coefficient [40].

Slowly varying signals are difficult to measure with piezoresistors due to 1/f noise at low frequency. By fabricating relatively large cantilevers in [21] with a high dopant concentration and large number of carriers, we reduced the 1/f corner frequency to below 1 Hz. Four active piezoresistors were included at the base of the cantilever in a full-bridge Wheatstone bridge configuration, and an integrated force resolution of 100 pN was realized between 0.1 Hz and 100 Hz (Figure 6). These devices are packaged with parylene and gold functional surfaces to bind reactive chemical species.

CONCLUSIONS

In summary, piezoresistive silicon transducers are widely used in MEMS for their simple fabrication, ease of integration and low-cost. Piezoresistive cantilevers can be readily fabricated at the micro- and nanoscale for high performance force sensing. We have presented an overview of piezoresistive cantilever design and optimization and summarized several example applications.

Cantilever design must balance the competing requirements of low noise and high sensitivity in order to achieve optimized performance.

ACKNOWLEDGEMENTS

Fabrication work was performed in part at the Stanford Nanofabrication Facility (a member of the National Nanotechnology Infrastructure Network) supported by the National Science Foundation (NSF) under Grant ECS-9731293, its lab members, and the industrial members of the Stanford Center for Integrated Systems. This work was supported by the National Institutes of Health under grant EB006745, and the NSF under grants ECS-0449400, ECS-0425914, PHY-0425897, CTS-0428889 and ECCS-0708031. Any opinions, findings, and conclusions or recommendations expressed in this material are those of the authors and do not necessarily reflect the views of the NSF or NIH. JCD was supported in part by a National Defense Science and Engineering Graduate (NDSEG) Fellowship and an NSF Graduate Research Fellowship. S-JP was supported by a Samsung fellowship.

References

1. A. Barlian, W.T. Park, J. Mallon, A. Rastegar, B. Pruitt, Review: Semiconductor piezoresistance for microsystems, Proceedings of the IEEE **97**(3), 513 (2009)

2. O. Hansen, A. Boisen, Noise in piezoresistive atomic force microscopy, Nanotechnology **10**, 51 (1999)

3. J. Harley, T. Kenny, 1/f noise considerations for the design and process optimization ofpiezoresistive cantilevers, Microelectromechanical Systems (2000)

4. X. Yu, J. Thaysen, O. Hansen, A. Boisen, Optimization of sensitivity and noise in piezoresistive cantilevers, Journal of Applied Physics (2002)

5. A. Merlos, J. Santander, M. Alvarez, F. Campabadal, Optimized technology for the fabrication of piezoresistive pressure sensors, Journal Of Micromechanics And Microengineering **10**, 204 (2000)

6. B. Bae, B. Flachsbart, K. Park, M. Shannon, Design optimization of a piezoresistive pressure sensor considering the output signal-to-noise ratio, Journal Of Micromechanics And Microengineering **14**, 1597 (2004)

7. C. Pramanik, H. Saha, U. Gangopadhyay, Design optimization of a high performance silicon mems piezoresistive pressure sensor for biomedical applications, Journal Of Micromechanics And Microengineering **16**, 2060 (2006)

8. Z. Wang, Y. Xu, Design and optimization of an ultra-sensitive piezoresistive accelerometer for continuous respiratory sound monitoring, Sensor Letters **5**, 450 (2007)

9. G. Villanueva, J. Plaza, J. Montserrat, F. Perezmurano, J. Bausells, Crystalline silicon cantilevers for piezoresistive detection of biomolecular forces, Microelectronic Engineering p. 4 (2008)

10. S.J. Park, M.B. Goodman, B.L. Pruitt, Analysis of nematode mechanics by piezoresistive displacement clamp, Proceedings of the National Academy of Sciences **104**(44), 17376 (2007)

11. G. Binnig, C. Quate, C. Gerber, Atomic force microscope, Physical Review Letters (1986)

12. F. Goericke, W. King, Modeling piezoresistive microcantilever sensor response to surface stress for biochemical sensors, Sensors Journal (2008)

13. M. Tortonese, R. Barrett, C. Quate, Atomic resolution with an atomic force microscope using piezoresistive detection, Applied Physics Letters (1993)

14. S.C. Minne, J.D. Adams, G. Yaralioglu, S.R. Manalis, A. Atalar, C.F. Quate, Centimeter scale atomic force microscope imaging and lithography, Applied Physics Letters (1998)

15. R. Ried, H. Mamin, B. Terris, L. Fan, D. Rugar, 5 mhz, 2 n/m piezoresistive cantilevers with incisive tips, Solid State Sensors and Actuators (1997)

16. C. Hagleitner, A. Hierlemann, D. Lange, A. Kummer, N. Kerness, O. Brand, H. Baltes, Smart single-chip gas sensor microsystem, Nature **414**(6861), 293 (2001)

17. J.C. Doll, S.J. Park, B.L. Pruitt, Design optimization of piezoresistive cantilevers for force sensing in air and water, Journal of Applied Physics **106**(6), 064310 (2009)

18. S.J. Park, J.C. Doll, A.L. Rastegar, B.L. Pruitt, Piezoresistive cantilever performance - part ii: Optimization, Journal of Microelectromechanical Systems (2009)

19. J. Harley, T. Kenny, High-sensitivity piezoresistive cantilevers under 1000 angstroms thick, Appl. Phys. Lett (1999)

20. J. Richter, J. Pedersen, M. Brandbyge, E.V. Thomsen, O. Hansen, Piezoresistance in p-type silicon revisited, Journal of Applied Physics **104**(2), 023715 (2008)

21. J.R. Mallon, A.J. Rastegar, A.A. Barlian, M.T. Meyer, T.H. Fung, B.L. Pruitt, Low 1/f noise, full bridge, microcantilever with longitudinal and transverse piezoresistors, Applied Physics Letters **92**, 3508 (2008)

22. J. Doll, B. Petzold, P. Ghale, M. Goodman, B. Pruitt, High frequency force sensing with piezoresistive cantilevers pp. 1928–1931 (2009)

23. M. Tortonese, Force sensors for scanning probe microcopy, Ph.D. dissertation, Dept. Appl. Phys., Stanford University (1993)

24. S.J. Park, J.C. Doll, B.L. Pruitt, Piezoresistive cantilever performance - part i: Analytical model for sensitivity, Journal of Microelectromechanical Systems (2009)

25. S.J. Park, B. Petzold, M. Goodman, B. Pruitt, Piezoresistive cantilever-based force-clamp system for the study of mechanotransduction in c. elegans, Proceedings of MEMS 2009 pp. 188–191 (2009)

26. S.D. Senturia, *Microsystem design* (2000)

27. G. Masetti, M. Severi, S. Solmi, Modeling of carrier mobility against carrier concentration in arsenic-, phosphorus-, and boron-doped . . . , Electron Devices (1983)

28. F. Hooge, 1/f noise sources, Electron Devices (1994)

29. B.C. Petzold, S.J. Park, P. Ponce, M.B. Goodman, B.L. Pruitt, The contribution of body wall muscles to c. elegans body mechanics determined using piezoresistive microcantilevers, Proceedings of microTAS 2009 pp. 1306–1308 (2009)

30. B.W. Chui, T.W. Kenny, H.J. Mamin, B.D. Terris, D. Rugar, Independent detection of vertical and lateral forces with a sidewall-implanted dual-axis piezoresistive cantilever, Applied Physics Letters **72**(11), 1388 (1998)

31. A. Partridge, J. Reynolds, B. Chui, E. Chow, A. Fitzgerald, L. Zhang, N. Maluf, T. Kenny, A high-performance planar piezoresistive accelerometer, Microelectromechanical Systems, Journal of **9**(1), 58 (2000)

32. A.A. Barlian, S.J. Park, V. Mukundan, B.L. Pruitt, Design and characterization of microfabricated piezoresistive floating element-based shear stress sensors, Sensors and Actuators A: Physical **134**(1), 77 (2007)

33. A. Barlian, N. Harjee, V. Mukundan, T. Fung, S.J. Park, B. Pruitt, Sidewall epitaxial piezoresistor process for in-plane sensing applications, Micro Electro Mechanical Systems (2008)

34. G. Hill, D. Soto, S. Lue, A. Peattie, R. Full, T. Kenny, Investigating the role of orientation angle on gecko setae adhesion using a dual-axis mems force sensor, Proceedings of Transducers 2007 pp. 2263–2266 (2007)

35. N. Harjee, A. Garcia, M. Knig, J. Doll, D. Goldhaber-Gordon, B. Pruitt, Coaxial tip piezoresistive scanning probes for high-resolution electrical imaging, Proceedings of MEMS 2010 (2010)

36. M. Topinka, B. LeRoy, S. Shaw, E. Heller, R. Westervelt, K. Maranowski, A. Gossard, Imaging coherent electron flow from a quantum point contact, Science **289**(5488), 2323 (2000)

37. G. Wu, H. Ji, K. Hansen, T. Thundat, R. Datar, R. Cote, M.F. Hagan, A.K. Chakraborty, A. Majumdar, Origin of nanomechanical cantilever motion generated from biomolecular interactions, Proceedings of the National Academy of Sciences **98**(4), 1560 (2001)

38. R. Mukhopadhyay, M. Lorentzen, J. Kjems, F. Besenbacher, Nanomechanical sensing of dna sequences using piezoresistive cantilevers, Langmuir **21**(18), 8400 (2005)

39. Q.T. Trinh, G. Gerlach, J. Sorber, K.F. Arndt, Hydrogel-based piezoresistive ph sensors: Design, simulation and output characteristics, Sensors and Actuators B: Chemical **117**(1), 17 (2006)

40. F. Goericke, W. King, Modeling piezoresistive microcantilever sensor response to surface stress for biochemical sensors, Sensors Journal, IEEE **8**(8), 1404 (2008)